J Appl Electrochem (2014) 44:675–682
DOI 10.1007/s10800-014-0677-z

RESEARCH ARTICLE

Electrochemical study of TiO_2 modified with silver nanoparticles upon CO_2 reduction

Luisa F. Cueto-Gómez · Nora A. Garcia-Gómez · Hugo A. Mosqueda · Eduardo M. Sánchez

Received: 16 August 2013 / Accepted: 3 February 2014 / Published online: 19 February 2014

Abstract A systematic cyclic voltammetry (CV) and electrochemical impedance spectroscopy (EIS) study on titanium dioxide (TiO_2) and silver–TiO_2 surfaces was performed in order to decouple electrochemical reduction processes of carbon dioxide in aqueous solutions. CV studies indicate cathodic current increase on Ag–TiO_2 compared to bare TiO_2 surfaces. An equivalent circuit based on transmission line model was applied in order to adjust EIS data, and a modification of this model was made to account for Ag particle interaction with the electrolyte solution. Electrochemical processes were then decoupled upon applied potential where the role of TiO_2 surface states was identified and separated from (a) silver reduction, (b) electronic transport on TiO_2, and (c) charge transfer on TiO_2 and Ag surfaces. The Ag–electrolyte interface impedance has considerably lower values than the TiO_2–electrolyte interface, suggesting that the silver particles may be considered as favorable reaction sites for the electrochemical reduction of water and carbon dioxide.

Keywords Electrochemical impedance spectroscopy · Transmission line model · Titanium dioxide · Carbon dioxide · Electrochemical reduction

1 Introduction

There is great interest on reducing air contamination due to industrial processes and automotive transportation because they both use energy sources such as oil, coal, and natural gas [1]. Their combustion results in several consequences to the environment such as the emission of greenhouse gases [2], of which carbon dioxide (CO_2) has the greatest concentration and 35 % is due to emissions from fossil fuel combustion and is receiving special attention because of it. Several approaches have been addressed in order to diminish such issues, for example, the generation of high-energy products [3] or total substitution [4]. The electrocatalytic reduction of carbon dioxide has been extensively studied [5], particularly in the gas phase. In aqueous systems, the electrochemical reduction of CO_2 has been reported using TiO_2 instead of traditional metallic electrodes by Monnier et al. [6]. In their work, they propose the formation of hydrogen gas during carbon dioxide electroreduction and surface reduction of Ti(IV) to Ti(III). Nevertheless, the electrochemical reduction of CO_2 on TiO_2 surfaces [7] or nanotubes [8] has been briefly studied. On the other hand, photoreduction of CO_2 in the presence of TiO_2 has been approached in a variety of experimental situations [9]. Also, the photoreduction of CO_2 by TiO_2 is enhanced by metallic silver [10]. Electrochemical impedance spectroscopy (EIS) is a valuable technique that presents the opportunity to separate electrochemical processes according to their reaction times. However, porous semiconductor electrodes such as TiO_2 deposited on glass slides present a rather complex behavior. Levie [11], and most recently Fabregat-Santiago et al. [12], proposed interesting ladder-like and transmission line equivalent circuit models to account for thin-layer porous surfaces where charge transport, faradic reactions, and surface polarization are present through the porous structure and are particularly coupled. In the case of a porous TiO_2 semiconductor, we may also consider the possibility of charge storage by the filling out of partially empty surface states (SSs) [13]. At

L. F. Cueto-Gómez · N. A. Garcia-Gómez · H. A. Mosqueda · E. M. Sánchez (✉)
Universidad Autónoma de Nuevo León, Av. Universidad s/n, Cd. Universitaria, 66450 San Nicolás de los Garza, NL, Mexico
e-mail: eduardo.sanchezcv@uanl.edu.mx

this point, we believe that there is an opportunity to enrich previous electrochemical CO_2 studies by conducting a variety of EIS experiments toward the reduction of carbon dioxide in aqueous media using a thin layer of TiO_2 as the working electrode and to extend this study with the incorporation of small silver particles on the surface. To the authors' best knowledge, there are no similar studies reported in the literature.

2 Experimental

Details of sol–gel deposition of TiO_2 over conductive glass slides and electrochemical deposition of silver particles over TiO_2 surfaces are published elsewhere [14, 15]. The electrolyte solution was a 0.5 M KCl deaerated DI aqueous solution (passed through dry nitrogen flow for 30 min to remove oxygen traces). A second solution was prepared by using same preparation, through which carbon dioxide (99.99 % pure) was passed for 60 min to saturate it. We used a 3-electrode electrochemical system for the reduction of carbon dioxide. TiO_2/FTO and Ag/TiO_2/FTO were selected as working electrodes (E_w), Ag/AgCl was chosen as the reference electrode (E_{ref}, from Bioanalytical Systems), and platinum wire mesh (2 × 2 cm) was used as an auxiliary electrode (E_{AUX}). Cyclic voltammetry (CV) was performed using a Gamry Instruments potentiostat (PCI4-750, equipped with a frequency response analyzer for EIS spectroscopy), and potential sweeps were performed on a typical 250 mV s^{-1} speed from potential at null current ($E_{i=0}$) until −0.9 V versus reference electrode through several cycles on electrolyte solution with and without electroactive species (saturated CO_2), and we also tested the use of deposited silver particles (250 nm average size) over TiO_2/FTO surfaces versus bare TiO_2/FTO samples.

For EIS experiments, we use same electrode configuration and solution preparation as was in the case for CV studies, previously discussed. Once the electrodes were immersed in the electrolyte solution, we wait for about 5 min to let open circuit voltage (OCV) to stabilize. Then we applied a sinusoidal voltage signal of 5 mV over a range of frequencies from 50 mHz to 100 kHz. After the scan was performed, we waited another 5 min to let OCV to stabilize. Then, a direct current potential (V_{DC}) was applied. After 5 min of stabilization, a new frequency scan was performed using a sinusoidal perturbation of 5 mV. This process was repeated varying the applied V_{DC} within a range of 0 to −1.2 V versus (Ag|AgCl). The experimental data obtained were analyzed with the program *ZSimpWin* 3.21 of EChem software adjusted to an equivalent circuit for a porous electrode based on transmission lines (TLs), initially proposed by Levie [11] and subsequently applied by Fabregat-Santiago et al. [12]. For proper adjustment of

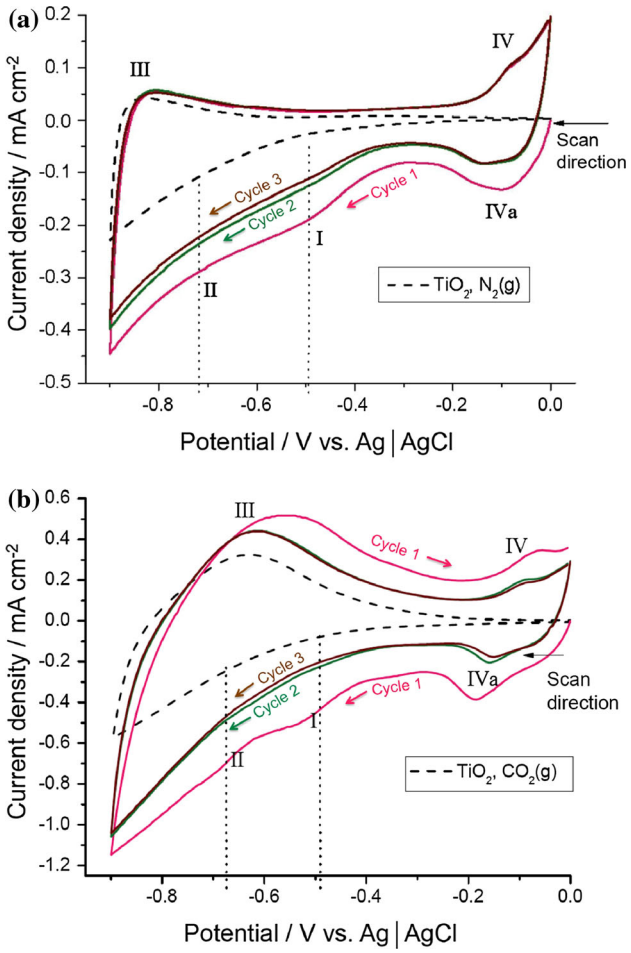

Fig. 1 Comparative CV of TiO_2/FTO (*dotted line*) and Ag/TiO_2/FTO (*solid lines*) electrodes in saturated solutions of **a** N_2(g) and **b** CO_2(g). E_{ref}: Ag|AgCl, E_{AUX}: Pt(s), scan rate = 250 mV s^{-1}

results to an electrical equivalent circuit, we consider the calculation of the goodness of fit of experimental data through the Chi-square (χ^2) with accepting values of 10^{-5}–10^{-6}.

3 Results and discussion

In Fig. 1, we present CV runs (first three cycles) performed on TiO_2/FTO (dotted line) and Ag–TiO_2/FTO (solid lines) electrodes in saturated solutions of nitrogen (Fig. 1a) and carbon dioxide (Fig. 1b). CV run on the TiO_2/FTO electrode initiated at open circuit potential until −0.9 V versus Ag|AgCl on both solutions; meanwhile, on the Ag–TiO_2/FTO electrode, initial potential was −0.3 V to avoid the reoxidation of small silver particles already deposited on the TiO_2 surface. In Fig. 1a, we show the case of N_2-(g) saturated solutions where event (I) is due to the effect of small silver particle deposition as one can observe a marked increase in current density on the Ag–TiO_2/FTO

electrode versus the TiO_2/FTO (dotted line) electrode at −0.5 V versus Ag/AgCl. This event will be considered, upon later EIS analysis, as the fulfillment of surface states of TiO_2. Event II (−0.72 V) is considered as the hydrogen evolution during the reduction of superficial Ti ions [16]. At this potential, we observe a 160 % increase in current density with the Ag–TiO_2/FTO compared to the TiO_2/FTO electrode, and faradic events are favored. Event III (−0.84 V) is considered as a reoxidation [17] of reduced species on event II and is considered a slow and irreversible process. Events IV and IVa correspond to a redox pair associated with the behavior of deposited small silver particles according to the following redox reaction:

$$Ag^{+} + e^{-} \leftrightarrow Ag^{0}$$

In Fig. 1b, we display the case of CO_2(g) saturated solutions. We observe similar events with N_2(s) with small displacements, which can be attributed to the modified pH media (according to the formation of carbonic acid: $CO_2(ac) + H_2O \leftrightarrow H_2CO_3$) [18]. Event I displays a current density increase of 460 % in the Ag–TiO_2/FTO electrode versus TiO_2/FTO, which is attributed to a strong interaction of small silver particles with CO_2, and is also considered the initial step of charge transfer through silver surface. In event II, we observe a displacement toward less negative potentials and a current density increase of 160 %. Both events indicate a positive effect in a general increase in current density (and charge transfer indeed) toward the electroactive species in solution (water and carbon dioxide). There are no significant changes in electrochemical potentials at peak III due to electrode modification, but there is a potential displacement of about 20 mV on the less negative direction when CO_2(g) is added. On the other side, current density on event III is increased by about 30 % using the Ag–TiO_2/FTO electrode, which is accounted for the increase in carbon dioxide electroreduction compared to the TiO_2/FTO electrode. The presence of CO_2 in IV and IVa events reflects a 150 % raise in current density with respect to the N_2(g) solution, indicating that CO_2 reduction is favored by the electrode modification and there is an active participation of small silver particles in the faradic process. In order to establish the degree to which CO_2 reduction is increased compared to H_2O reaction, a series of electrochemical impedance spectroscopies was performed; this is discussed next.

As mentioned earlier, several electron transfer processes are carried out in porous electrodes [15]. Electrical transfer and ion transport processes may occur simultaneously, but they can be isolated by EIS techniques. In case of porous electrodes, the preferred electrical equivalent circuit is based on a TL model, as shown in Fig. 2 [19]. The model used in this work is the R_SX electrical equivalent circuit, where the TL element called X is composed of an infinite array of R_{TiO_2} series resistances connected with an interfacial impedance composed of a charge transfer resistance, R_{ct}, in parallel with a constant phase element, Q_{if}. Particularly, R_S is the electrolyte resistance, R_{TiO_2} is considered the electron transport impedance through the TiO_2 porous material and R_{ct} is associated with the interface charge resistance toward the solution, and they can be associated with the faradaic processes of the electroactive species in the electrolyte. This model assumes the complete filling of the pores with the electrolyte solution.

For a porous electrode in which faradaic and surface polarizations are involved, the following [19] equation for TL impedance (Z_X) applies

$$Z_X = \left[\frac{R_{TiO_2}R_{ct}}{1+\left(\frac{i\omega}{\omega_{if}}\right)^{\beta}}\right]^{\frac{1}{2}} \coth\left(\left(\frac{\omega_{if}}{\omega_L}\right)^{\frac{\beta}{2}}\left[1+\left(\frac{i\omega}{\omega_{ct}}\right)^{\beta}\right]^{\frac{1}{2}}\right)$$

where ω_L is the intramaterial frequency $(\omega_L = 1/(R_{TiO_2}Q_{if})^{1/\beta})$ through the porous TiO_2 and ω_{if} is the interfacial frequency $\left(\omega_{if} = 1/(R_{ct}Q_{if})^{1/\beta}\right)$. When $\omega_L > \omega_{if}$, we interpreted as faster electronic transfer in comparison to the interfacial charge transfer. Also, Q_{if} can be associated to the disperse capacitance due to irregular TiO_2 surface. Parameter β is associated with the dispersion parameter of the ideal surface charge storage, and its value lies within $0 < \beta < 1$.

4 TiO_2/FTO electrode immersed in saturated CO_2 electrolyte solution

In Fig. 3, we present the Nyquist (a) and Bode (b) plots of the impedance experiments from −0.10 to −0.55 V (vs. Ag/AgCl) applied potential of the CO_2 saturated electrolyte solution (0.5 M KCl) using the TiO_2/FTO electrode. Fitted lines are calculated using the TL R_SX equivalent circuit model. In Fig. 3a, we observe a predominantly capacitive behavior where the real impedance (Z'_X) is far below the imaginary part ($|Z'_X|$) indicating electrode polarization. The inset in Fig. 3a is an amplification of the Nyquist plot where we observe electronic transport processes through the material at high frequencies showing its characteristic ω_L "elbow," which is related to electron diffusion through the porous TiO_2 film [20]. Calculated R_{TiO_2} values are well below calculated R_{ct} values, indicating fast electronic charge transfer with slower charge transfer processes through the electrode–electrolyte interface. The sigmoidal shape of the phase-Bode plot (Fig. 3b) with values near to zero at high frequencies and increasing up to 80° at lower frequencies and the absolute impedance (inset Fig. 3b), decreasing at high frequencies, confirm the nature of

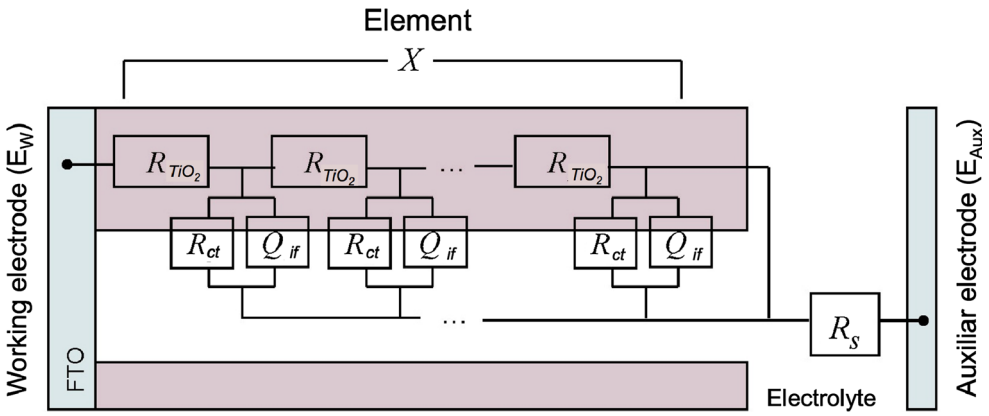

Fig. 2 Circuit electrical circuit based on a transmission line model (TLM) for a porous electrode R_SX

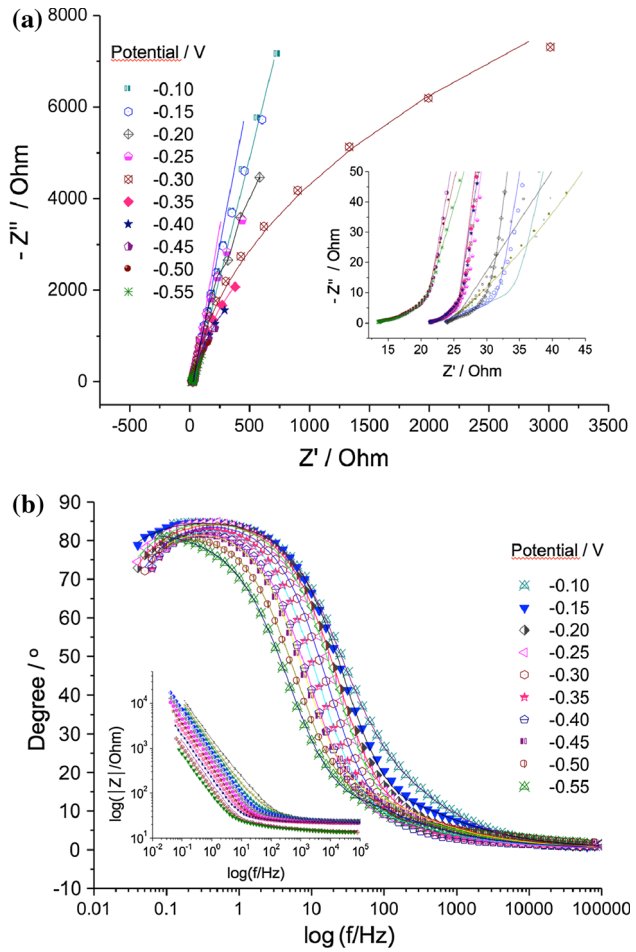

Fig. 3 **a** Nyquist and **b** Bode plot for Region I (−0.10 to −0.55 V) adjusted with TLM R_SX. E_w: TiO_2/FTO, E_{ref}: Ag|AgCl, and E_{AUX}: Pt(s) in 0.5 M KCl in water saturated with CO_2(g)

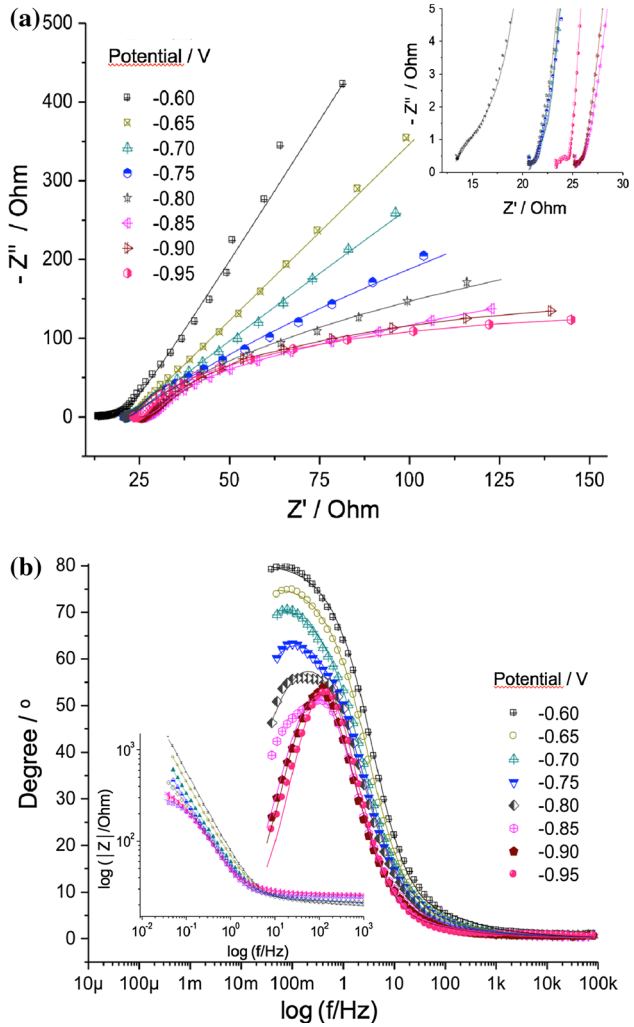

Fig. 4 **a** Nyquist and **b** Bode plot for Region II (−0.60 to −0.95 V) adjusted with TLM *RSX*. E_w: TiO_2/FTO, E_{ref}: Ag|AgCl, and E_{AUX}: Pt(s) in 0.5 M KCl in water saturated with CO_2(g)

electrode polarization within this potential range (called region I from now on).

In Fig. 4, we present the Nyquist (a) and Bode (b) plots of the impedance experiments under −0.60 to −0.95 V (vs. Ag/AgCl) applied potential of the CO_2 saturated electrolyte solution (0.5 M KCl) using the TiO_2/FTO electrode. Fitted lines are calculated using the TL R_SX equivalent circuit model. Here, we can observe a superficial polarization as well as the beginning of charge transfer processes. In the Nyquist plot, we observe that at lower negative values

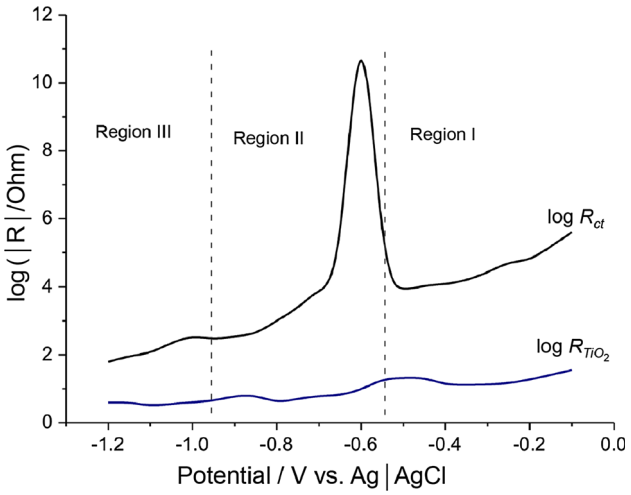

Fig. 5 Calculated electronic resistance (R_{TiO_2}) and charge transfer resistance (R_{ct}) through the electrode–electrolyte interface versus applied potential. Data were adjusted using TLM R_SX

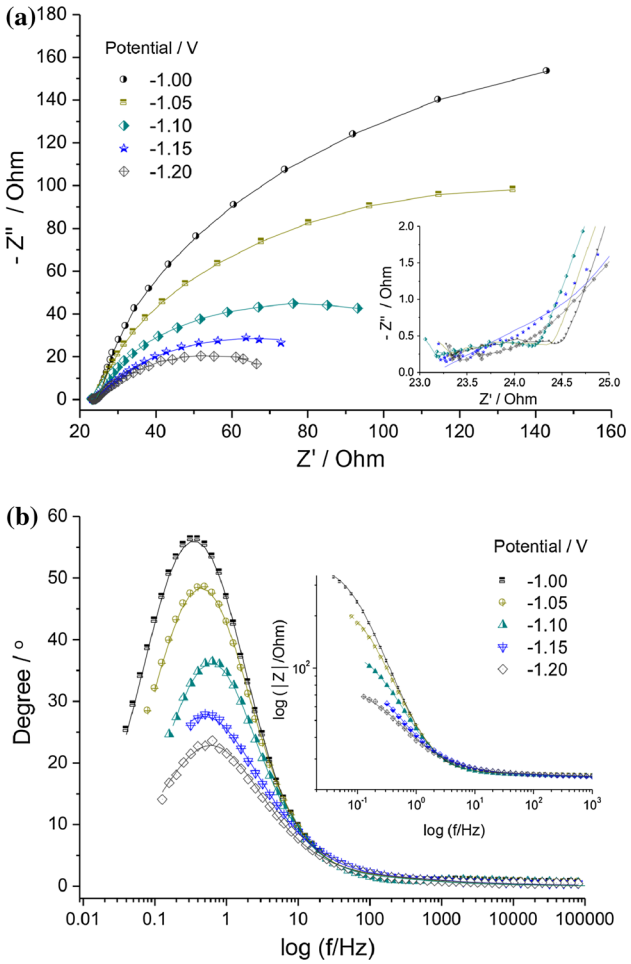

Fig. 6 **a** Nyquist and **b** Bode plot for Region III (−1.0 to −1.2 V) adjusted with TLM R_SX. E_w: TiO_2/FTO, E_{ref}: AgIAgCl, and E_{AUX}: Pt(s) in 0.5 M KCl in water saturated with CO_2(g)

Bode plots start to change toward a semicircular shape, ($0 < Z'_X < 125\ \Omega$, $0 < |Z'_X| < 400\ \Omega$), indicating a change in transport behavior. We can also observe the characteristic "elbow" for porous materials in Fig. 4a (inset). In the Bode plot (Fig. 4b), we observe changing shapes from sigmoidal to dumb bell-like contours starting at −0.80 V, confirming diffusion transport throughout the electrode–electrolyte interface. These results agree with the current increases in CV experiments (Fig. 1). To distinguish it from region I results, this potential range will be known as region II. Calculated R_{TiO_2} and R_{ct} values, using the TL $R_{elect}X$ equivalent circuit model, toward the whole potential sweep is presented in Fig. 5, where we observe a transition in R_{ct} value when going from region I to region II with a marked increase starting at −0.55 to −0.60 V and increasing up to six orders of magnitude, where we interpret it as the filling out of TiO_2 surface states. When potential is increased in the cathodic direction, log R_{ct} values are lowered up to two orders of magnitude compared to region I where we denote the end of region II (−0.95 V).

We consider region III (−1.0 to −1.20 V) to be a faradic region of electrochemical species (CO_2 and water), as indicated by CV experiments and corroborated on Nyquist and Bode plots (Fig. 6). Toward lower potential values, the Nyquist plots take a more circle-like shape ($0 < Z'_X < 140\ \Omega$, $0 < |Z'_X| < 150\ \Omega$), indicating a charge transfer process, which is confirmed by lowering values of log R_{ct} on negative potential bias (Fig. 5). Zooming on the Nyquist plot (Fig. 6a, inset) displays, once again, the characteristic "elbow" for mesoporous materials. The phase-Bode plot (Fig. 6b) shows a bell shape with a tendency of diminishing peak height toward less negative potentials, which is interpreted as an increase in charge transfer processes and corroborated on current increases in CV experiments. We need to point out that log R_{TiO_2} values have small changes but have a tendency to diminish (see Fig. 5) on the negative side, indicating a general increase in electrical transfer on TiO_2 porous electrode through more negative potentials.

5 Ag–TiO_2/FTO electrode immersed in saturated CO_2 electrolyte solution

To account for the deposition of small silver particles, we propose a modification of the transmission line R_SX electrical equivalent circuit model, since it is ineffective when fitting Ag–TiO_2/FTO electrode experiments. We consider that an Ag particle attached to the TiO_2 surface (Fig. 7) will behave as a silver particle–TiO_2 surface impedance of $R_{Ag-If}Q_{Ag-If}$. Since this particle has a rather small surface compared to the wall pore, we can neglect the effect of the

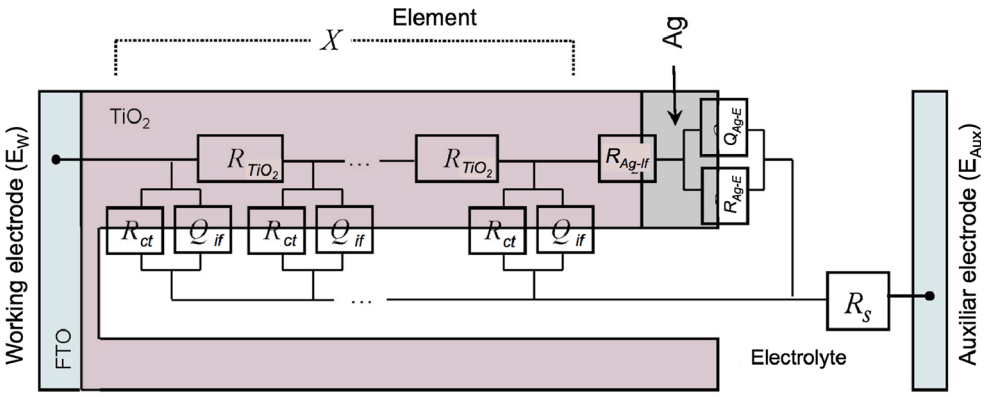

Fig. 7 Circuit electrical circuit based on a transmission line model (TLM) for a porous electrode with silver particles deposited over the TiO_2 surface represented by $R_S(X(R_{Ag-If}(R_{Ag-E}Q_{Ag-E})))$

silver particle charge storage (Q_{Ag-If}). Since silver is a good electronic conductor, we can also neglect the effect of the electronic transfer within the metallic material. On the silver–electrolyte interface, we also have an interface with an impedance of $R_{Ag-E}Q_{Ag-E}$, where preliminary fittings account for both electrical elements. Therefore, the working model selected to study these electrode–electrolyte interactions was $R_S(X(R_{Ag-If}(R_{Ag-E}Q_{Ag-E})))$, as displayed in Fig. 7. The rest of the equivalent electrical elements on impedance model *X* has been explained earlier.

In Fig. 8, we present the Nyquist (a) and Bode (b) plots of the impedance experiments under −0.30 to −1.20 V (vs. Ag/AgCl) applied potential on CO_2 saturated electrolyte solution (0.5 M KCl) and Ag–TiO_2/FTO electrode. Fitted lines are calculated using the TL $R_S(X(R_{Ag-If}(R_{Ag-E}Q_{Ag-E})))$ equivalent circuit model. Here, we can observe a superficial polarization at the beginning of potential sweep with impedances in the range of 400–800 Ω (−0.3 and −0.5 V, respectively). However, when starting at −0.6 V and until reaching −1.2 V, we observe a decrement in impedances down to 100–200 Ω, indicating a change in transport behavior. We can also observe the characteristic high-frequency "elbow" in Fig. 8a (inset), particularly below −0.6 V versus Ag/AgCl. The phase-Bode plot (Fig. 8b) displays a capacitive behavior at –0.4 V with a phase displacement up to 80°. From −0.6 V and marked at −0.7 V and so on, we can observe bell-shaped curves at lower frequencies, suggesting a diffusion transport at the interface, as corroborated by CV experiments. In Fig. 9, we plot the calculated logarithmic values of the calculated electron transport impedance through the TiO_2 porous material (R_{TiO_2}), the charge transfer resistance (R_{ct}) of the porous interface, and the new interface resistance (R_{Ag-E}) associated with the silver particle-interface charge transfer resistance. Calculated values for silver particle–TiO_2 surface impedance (R_{Ag-If}) are quite low, indicating good contact, and are not included in Fig. 9. Here, we observe small changes in log R_{TiO_2} values, particularly at −0.4 V where electric transport on TiO_2 is more favorable for

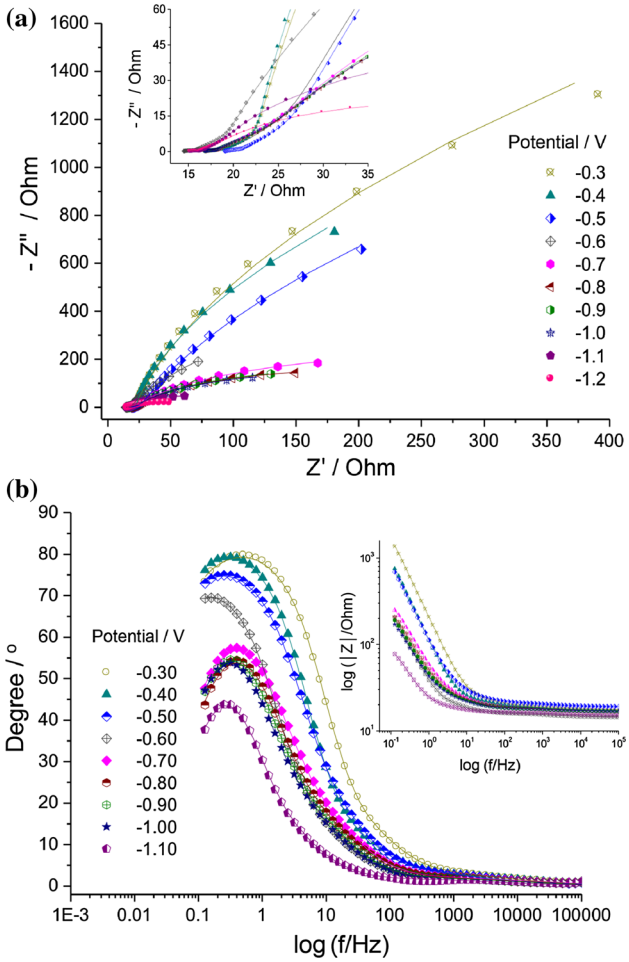

Fig. 8 **a** Nyquist and **b** Bode plot (−0.03 to −1.2 V) adjusted with TLM $R_S(X(R_{Ag-If}(R_{Ag-E}Q_{Ag-E})))$. E_w: Ag/TiO_2/FTO, E_{ref}: Ag|AgCl, and E_{AUX}: Pt(s) in 0.5 KCl M in water saturated with CO_2(g)

fulfillment of the SS of the TiO_2 semiconductor. R_{Ag-E} displays lower values than R_{ct}, indicating that electrons are favorably conducted toward the silver–electrolyte interface rather than the TiO_2–electrolyte interface in the entire potential domain, suggesting an increased charge transfer

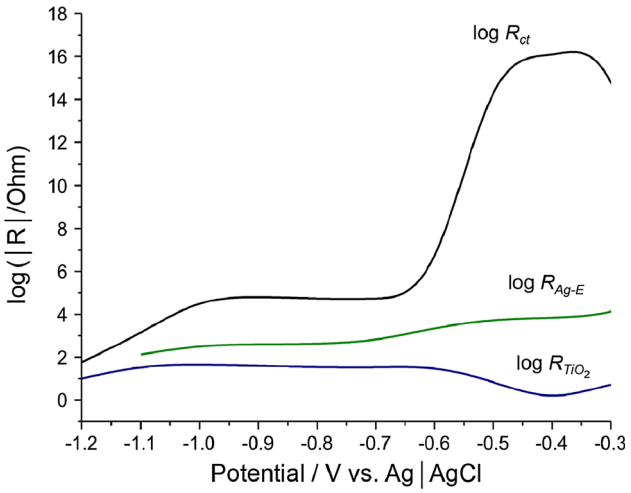

Fig. 9 Calculated electronic resistance (R_{TiO_2}), charge transfer resistance on the TiO_2–electrolyte interface (R_{ct}) and charge transfer resistance on the Ag–electrolyte interface (R_{Ag-E}) versus applied potential. Data were adjusted using TLM $R_S(X(R_{Ag-If}(R_{Ag-E}Q_{Ag-E})))$

to the electroactive species (CO_2 and water) in the electrolyte due to the small silver particle effect, as corroborated by CV experiments (see Fig. 1). On the other hand, as in the case for the TiO_2/FTO sole electrode, we observe a marked increase in log R_{ct} values, particularly between −0.3 and −0.6 V, as a corroboration of the filling out of TiO_2 SS.

Previous work on CO_2 electroreduction performed by Monnier et al. [6] suggested the reduction of Ti(IV) along hydrogen evolution and carbon dioxide reduction. Within this work, we proposed that before electrons become available to such electrochemical reduction processes, a certain amount of electrons should be used to fill out surface states within TiO_2 nanostructure therefore reducing the amount of electrons available for the electroactive species. With the incorporation of silver particles to the surface, we observe an increase on the cathodic current, and after EIS analysis, we propose the formation of preferable pathways through the TiO_2–Ag interface favoring the electron transfer toward better reduction processes.

6 Conclusions

A systematic EIS study on TiO_2/FTO and Ag/TiO_2/FTO surfaces was performed in order to decouple the electrochemical processes of CO_2 and the water electrochemical reduction taking place at these surfaces. CV results indicate a favorable effect of Ag particles deposited over TiO_2 surfaces on increasing cathodic reduction of electrochemical species. The obtained results can be well adjusted using a TL model for porous electrodes. For TiO_2/FTO, we observe fast electronic transport through the porous TiO_2 at high frequencies (low R_{TiO_2}), which is virtually unaffected by the applied potential; meanwhile, we observe slow TiO_2–electrolyte interface charge transport (high R_{ct}) at lower frequencies. Charge transport in CO_2 saturated solution is closely related to the applied potential. At low potentials, we notice a polarized surface (region I) behavior changing toward a faradaic region (III) at lower cathodic potentials with an intermediate regime (II), when electrons are being occupied upon SS filling out. For Ag/TiO_2/FTO, we detect fast electron transport through porous TiO_2 at high frequencies as well as slow charge transfer processes at lower frequencies. In addition, we recognize that the TiO_2–Ag interface presents fast electronic transport with low impedances; we also distinguish different charge transfer impedances that were assigned to the silver particle–electrolyte interface. The applied potential has a strong influence on TiO_2–electrolyte charge transfer resistance (as in the previous case), with values going really high on the −0.4 to −0.6 V range, suggesting the filling out of TiO_2 surface states. On the other hand, the resistance values of the TiO_2–Ag interface were rather low, indicating good contact. The Ag–electrolyte interface impedance has considerably lower values than the TiO_2–electrolyte interface, suggesting that the silver particles may be considered as favorable reaction sites for the electrochemical reduction of water and carbon dioxide.

Acknowledgments The authors express their thanks to the projects SEP-CONACyT #151587 and SENER-CONACyT #150111 for their support to this work. In addition, the support of the Universidad Autónoma de Nuevo León, Monterrey, México, under PAICyT programs is recognized.

References

1. Kindzierski WB, Small CC, Fang Y, Bari MdA, Hashisho Z (2012) Automotive wastes. Water Environ Res 84:1407–1431. doi:10.2175/106143012X13407275695247
2. Davis SJ, Caldeira K, Matthews HD (2010) Future CO_2 emissions and climate change from existing energy infrastructure. Science 329:1330–1333. doi:10.1126/science.1188566
3. Kumar B, Llorente M, Froehlich J, Dang T, Sathrum A, Kubiak CP (2012) Photochemical and photoelectrochemical reduction of CO_2. Annu Rev Phys Chem 63:541–569. doi:10.1146/annurev-physchem-032511-143759
4. Omae I (2006) Aspects of carbon dioxide utilization. Catal Today 115:33–52. doi:10.1016/j.cattod.2006.02.024
5. Genovese C, Ampelli C, Perathoner S, Centi G (2013) Electrocatalytic conversion of CO_2 to liquid fuels using nanocarbon-based electrodes. J Energy Chem 22:202–213. doi:10.1016/S2095-4956(13)60026-1
6. Monnier A, Augustynski J, Stalder C (1980) On the electrolytic reduction of carbon dioxide at TiO_2 and TiO_2–Ru cathodes. J Electroanal Chem Interfacial Electrochem 112:383–385. doi:10.1016/S0022-0728(80)80420-7
7. Zhang L, Wang J, Zhang H, Cai W (2010) A novel fabrication of RuO_2/TiO_2 nanofilms for electrocatalytic reduction of CO_2. Acta Chim Sinica 68:590–593

8. Qu J, Zhang X, Wang Y, Xie C (2005) Electrochemical reduction of CO_2 on RuO_2/TiO_2 nanotubes composite modified Pt electrode. Electrochim Acta 50:3576–3580. doi:10.1016/j.electacta.2004.11.061
9. Yui T, Tamaki Y, Sekizawa K, Ishitani O (2011) Photocatalytic reduction of CO_2: from molecules to semiconductors. Photocatalysis 303:151–184. doi:10.1007/128_2011_139
10. Kočí K, Matějů K, Obalová L, Krejčíková S, Lacný Z, Plachá D, Čapek L, Hospodková A, Šolcová O (2010) Effect of silver doping on the TiO_2 for photocatalytic reduction of CO_2. Appl Catal B 96:239–244. doi:10.1016/j.apcatb.2010.02.030
11. de Levie R (1963) On porous electrodes in electrolyte solutions: I. Capacitance effects. Electrochim Acta 8:751–780. doi:10.1016/0013-4686(63)80042-0
12. Fabregat-Santiago F, García Belmonte G, Bisquert J, Zaban A, Salvador P (2002) Decoupling of transport, charge storage, and interfacial charge transfer in the nanocrystalline TiO_2/electrolyte system by impedance methods. J Phys Chem B 106:334–339. doi:10.1021/jp0119429
13. Mora-Seró I, Bisquert J (2003) Fermi level of surface states in TiO_2 nanoparticles. Nano Lett 3:945–949. doi:10.1021/nl0342390
14. Cueto LF, Sánchez E, Torres-Martinez LM, Hirata GA (2005) On the optical, structural, and morphological properties of ZrO_2 and TiO_2 dip-coated thin films supported on glass substrates. Mater Charact 55:263–271. doi:10.1016/j.matchar.2005.05.004
15. Dávila-Martínez RE, Cueto LF, Sánchez EM (2006) Electrochemical deposition of silver nanoparticles on TiO_2/FTO thin films. Surf Sci 600:3427–3435. doi:10.1016/j.susc.2006.06.041
16. Lyon LA, Hupp JT (1999) Energetics of the nanocrystalline titanium dioxide/aqueous solution interface: 2009 approximate conduction band edge variations between $H_0 = -10$ and $H_- = +26$. J Phys Chem B 103:4623–4628. doi:10.1021/jp9908404
17. Augustynski J (1983) Comments on the paper on the electrolytic reduction of carbon dioxide at TiO_2 and other titanates by A.H.A. Tinnemans, T.P.M. Koster, D.H.M.W. Thewissen, C.W. De Kreuk and A. Mackor. J Electroanal Chem Interfacial Electrochem 145:457–460. doi:10.1016/S0022-0728(83)80100-4
18. Sullivan BP, Krist K, Guard HE (1993) Electrochemical and electrocatalytic reactions of carbon dioxide. Elsevier Science, New York
19. Bisquert J, García-Belmonte G, Fabregat-Santiago F, Ferriols NS, Bogdanoff P, Pereira EC (2000) Doubling exponent models for the analysis of porous film electrodes by impedance relaxation of TiO_2 nanoporous in aqueous solution. J Phys Chem B 104:2287–2298. doi:10.1021/jp993148h
20. Gimenez S, Dunn HK, Rodenas P, Fabregat-Santiago F, Miralles SG, Barea EM, Trevisan R, Guerrero A, Bisquert J (2012) Carrier density and interfacial kinetics of mesoporous TiO_2 in aqueous electrolyte determined by impedance spectroscopy. J Electroanal Chem 668:119–125. doi:10.1016/j.jelechem.2011.12.019